

EPP-Net: Extreme-Point-Prediction-Based Object Detection

Yang Yang^{1,2}, Min Li^{1,2}, Bo Meng^{1,2}, Zihao Huang^{1,2}, Junxing Ren^{1,2} and Degang Sun^{1,2}

¹Institute of Information Engineering, Chinese Academy of Sciences

²School of Cyber Security, Chinese Academy of Sciences

{yangyang1995, limin, renjunxing, sundegang}@iie.ac.cn, bit.meng@live.com,

Abstract

Object detection can be regarded as a pixel clustering task, and its boundary is determined by four extreme points (leftmost, top, rightmost, and bottom). However, most studies focus on the center or corner points of the object, which are actually conditional results of the extreme points. In this paper, we present a new anchor-free dense object detector, which directly regresses the relative displacement vector between each pixel and the four extreme points. We also propose a new metric to measure the similarity between two groups of extreme points, namely, Extreme Intersection over Union ($EIoU$), and incorporate this $EIoU$ as a new regression loss. Moreover, we propose a novel branch to predict the $EIoU$ between the ground-truth and the prediction results, and combine it with the classification confidence as the ranking keyword in non-maximum suppression. On the MS-COCO dataset, our method achieves an average precision (AP) of 39.3% with ResNet-50 and an AP of 48.3% with ResNeXt-101-DCN. The proposed EPP-Net provides a new method to detect objects and outperforms state-of-the-art anchor-free detectors.

1 Introduction

Object detection is a crucial prerequisite for many computer vision tasks, such as instance segmentation [He *et al.*, 2017] and multi object tracking [Wojke *et al.*, 2017]. It also plays an essential role in many downstream technologies, such as intelligent video analysis and autonomous driving. Benefiting from the excellent performance of anchors, the detection accuracy of one-stage [Redmon and Farhadi, 2017] and two-stage [Ren *et al.*, 2016] object detectors has substantially improved. However, these detectors rely excessively on predefined anchors, thus requiring fine-tuning when training, and lead to poor generalization performance. Anchor-free detectors [Tian *et al.*, 2019; Kong *et al.*, 2020] have recently drawn much attention for their simple design, great accuracy, and high speed. Generally, anchor-free detectors can be classified into **key-point-based prediction** and **dense prediction**.

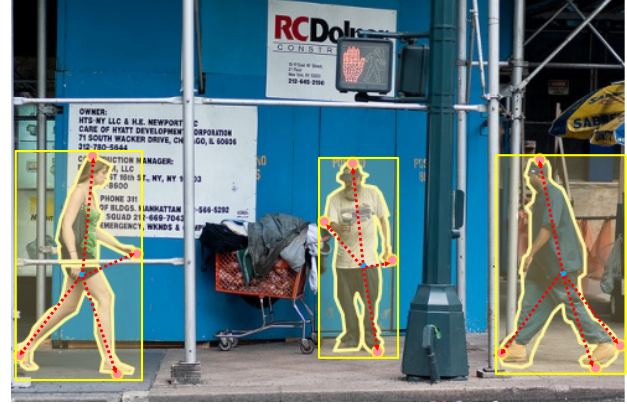


Figure 1: Illustration of EPP-Net predictions.

Key-point-based prediction. The location of an object is usually represented by the smallest enclosing rectangle called the bounding box (bbox). Nevertheless, not all objects can perfectly fit into a rectangle, such as objects with a tilted angle. CornerNet [Law and Deng, 2018] represents an object using a pair of corner points (top left and bottom right), whereas [Duan *et al.*, 2019] also predicts the center point besides corner points. ExtremeNet [Zhou *et al.*, 2019] argues that corner points usually lie outside the object and lack appearance features. Therefore, it utilizes the four extreme points and the center points to represent the object. Free from the limitations of the rectangular box, these key-point-based detectors surpass anchor-based detectors for the first time. However, they require post-processing to group key-points to the same instance, which slows down the overall computing speed. Moreover, *the boundary of an object is determined by four extreme points, the corner points and the center point are both conditional results*. Therefore, the extreme regions have more substantial location features than the other ones.

Dense prediction. FCN [Long *et al.*, 2015] powers various detectors to achieve high-precision dense prediction, such as FCOS [Tian *et al.*, 2019] and FoveaBox [Kong *et al.*, 2020]. In general, object detection algorithms process an image on the object level, whereas FCOS proves for the first time that the object detection task could also be solved in a per-pixel prediction fashion. This pixel-level-based detector provides a more fine-grained manner to understand an image. For each

pixel, FCOS predicts the relative distances from the four sides of the bbox. Compared with the four extreme points, *the bbox lacks the offsets’ supervision in the four boundary directions, making finding the real boundary of the objects, especially those with a large shape variance, more challenging.*

Motivation. Object detection involves classification and localization (bbox regression). However, there exists a misalignment between them. IoU-net [Jiang *et al.*, 2018] finds that some detection results with high classification confidence have coarse bbox predictions. *Therefore, taking classification confidence as the only criterion of detection results is not accurate enough.* BorderDet [Qiu *et al.*, 2020] utilizes border features to improve detection results. It also reveals that *the most important features for localization lie in the extreme point regions.*

In this paper, we provide **EPP-Net**, a simple yet effective fully convolutional one-stage object detection method, which densely predicts the relative displacement vector between each location and the four extreme points, as shown in Figure 1. We also propose a new evaluation metric, namely, Extreme Intersection over Union ($EIoU$), to measure the similarity between two groups of extreme points, and a new loss function, namely, Extreme IoU loss, tailored for this model. Moreover, we propose a new branch to predict the $EIoU$ between the extreme points and the matched ground-truth with the $EIoU$ servers as the localization confidence for each prediction result. By combining the predicted $EIoU$ with the classification confidence as the ranking keyword in non-maximum suppression (NMS), we show a considerable improvement in the detection results.

In summary, the contributions of this paper are as follows:

1. EPP-Net decomposes the detection task into extreme points prediction and classification. Compared with other key-point based methods, EPP-Net does not need a subsequent grouping process.
2. We propose $EIoU$, a normalized and scale-invariant evaluation metric, to measure the similarity between any two convex quadrilaterals or any two groups of extreme points. By incorporating $EIoU$ as the regression loss, namely, Extreme IoU loss ($EIoU$ loss), the accuracy with $EIoU$ loss can easily exceed that of Smooth- ℓ_1 loss by 1.4% without fine-tuning.
3. We present a $EIoU$ predictor to solve the misalignment problem between localization and classification. The predicted $EIoU$ serves as the localization confidence, and it is combined with the classification confidence as the ranking keyword in NMS. After appending this branch, the AP is improved by 0.5%. With the $EIoU$ -guided NMS, the AP is improved by 0.2%.

2 Related Work

2.1 Anchor-Free Object Detection

Current anchor-free detectors can achieve the same accuracy as anchor-based ones, with fewer hyperparameters and no complicated IoU calculations. Despite the fact that DenseBox [Huang *et al.*, 2015] and YOLOv1 [Redmon *et al.*, 2016]

are the earliest explorations of anchor-free models, DenseBox is not suitable for generic object detection, and the YOLO family added the anchor strategy in its subsequent versions. Therefore, these two methods are not included in the following discussions.

Key-point-based prediction. Key-point based detectors detect an object as one or several key-points and utilize post-processing methods to group the key points. CornerNet outputs the heatmaps of the top-left and bottom-right corners and an embedding vector for each key-point. In its grouping process, embeddings that have smaller Euclidean distances are grouped as the same instance. Based on CornerNet, [Duan *et al.*, 2019] adds center point prediction. In its grouping process, it also uses embedding vectors to group points. Each predicted bbox has a predefined central region and will be preserved only when the center point falls in this region. ExtremeNet predicts four extreme points and a center point for each object. In its grouping process, it uses a brute force method to enumerate all possible combinations. The box will be preserved only when the geometric center of the extreme points has a high response in the center point heatmap. The time complexities of these post-processing methods are $O(n^2)$, $O(n^2)$, and $O(n^4)$, respectively, which slow down the overall computing speed. Our EPP-Net directly predicts the relative displacement vector between each location and the four extreme points; thus, it does not need a grouping process.

Dense prediction. FSAF [Zhu *et al.*, 2019a] employs an extra anchor-free module on the anchor-based detector for detection and feature selection. FSAF calculates the total loss for each instance and selects the pyramid level with the minimal loss to learn the instance. FoveaBox predicts category-sensitive semantic maps for the object’s existing possibility and the bbox for each position that potentially contains an object. Our method outperforms them without the feature selection strategy and category-sensitive semantic maps. For FCOS, each location inside the object is a potential positive sample, and it directly predicts the relative distances from the four sides of the bbox to the location. It also utilizes a centerness branch to suppress classification results far from the center region. Compared with it, our EPP-Net combines the localization and classification confidence to select the best detection results, which is more reasonable. Moreover, Instead of regressing the four bounds of the bbox, the way EPP-Net predicts is more precise.

2.2 Localization and Classification Spatial Misalignment

Localization is a position-sensitive task, whereas classification is not because of its translation and scale invariance properties; that is, the position or scale change of features does not affect the classification results. Therefore, a spatial misalignment exists between them. TSD [Song *et al.*, 2020] proves that localization is boundary-sensitive, whereas classification is salient-area-sensitive. IoU-net utilizes an extra branch to predict the IoU between the detection results and ground-truth bboxes, and takes it as the ranking keyword in NMS. In contrast to IoU-net, first, EPP-Net is an anchor-free one-stage

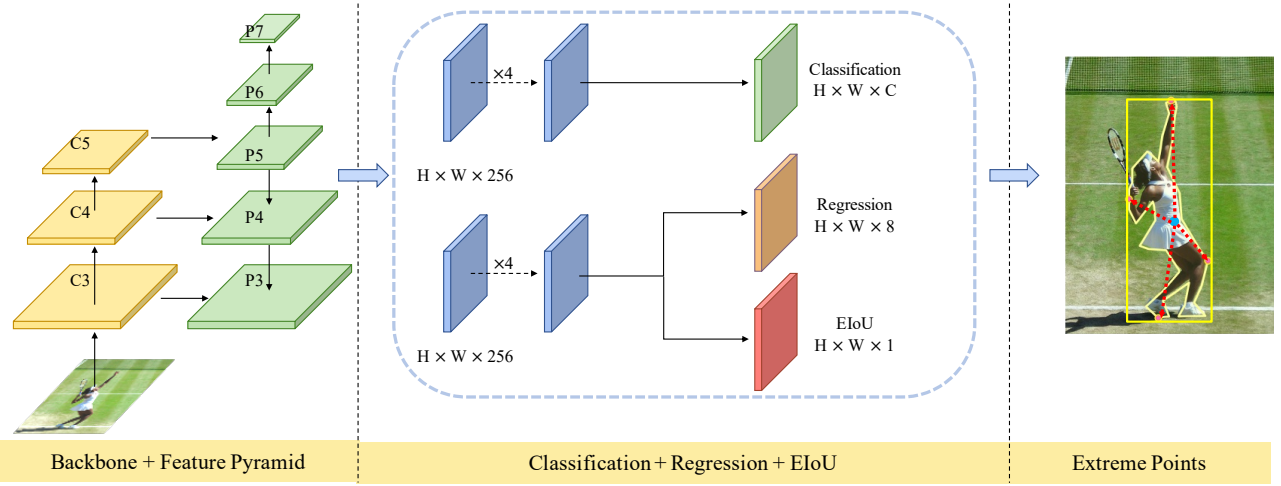


Figure 2: **Architecture of EPP-Net.** This network consists of a backbone, a feature pyramid network, and two branches, corresponding to classification and regression. For each pixel, EPP-Net outputs classification confidence, regression results, and $EIoU$.

detector. Second, EPP-Net predicts $EIoU$ instead of IoU as the localization confidence, which is tailored for this unique regression task. Finally, the localization confidence is combined with classification confidence, not just the localization confidence, to filter the detection results.

2.3 Regression Loss

ℓ_n -norm-based losses are widely used in bbox regression. However, they suffer from the scale imbalance problem, which means the loss value is affected by the scale of the bbox. IoU is an evaluation metric that measures the overlap between two bboxes. [Yu *et al.*, 2016] proposes IoU loss based on this metric, which also inherits IoU 's scale invariance. When the two bboxes do not overlap, IoU becomes 0 and cannot be optimized. Therefore, $GIoU$ loss [Rezatofighi *et al.*, 2019] is proposed to solve this problem. Standing on the shoulders of giants, we propose $EIoU$ loss to measure the similarity of two convex quadrilaterals.

3 Method

In this section, we briefly introduce the details of EPP-Net. We use FCOS as the baseline and ResNet-50 as the basic backbone. In EPP-Net, an object is detected as four extreme points (leftmost, top, rightmost, and bottom) by predicting the relative displacement vector in a per-pixel prediction fashion. We propose $EIoU$ as well as $EIoU$ loss for extreme point regression. Finally, we propose a novel $EIoU$ predictor for accurate key-point prediction.

3.1 Positive Sampling with Dynamic Radius

The extreme points ground-truth are defined as E , where $E = (x_1, y_1, x_t, y_t, x_r, y_r, x_b, y_b) \in \mathbb{R}^8$. Given a location (x, y) , if it falls into the target area of the ground-truth box, it is considered as a positive sample; otherwise, a negative sample. Let (c_x, c_y) be the center point of the ground-truth box, and s_i [Tian *et al.*, 2019] be the stride of feature map i . The target area is defined as $(c_x - s_i \times r_x, c_y - s_i \times r_y, c_x + s_i \times r_x, c_y + s_i \times r_y)$.

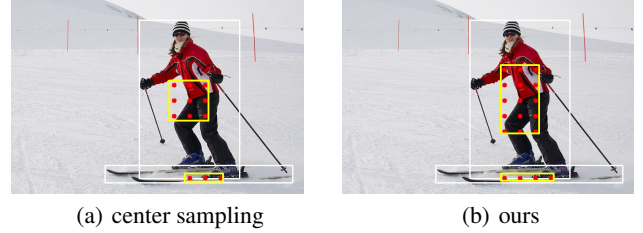


Figure 3: **Positive Sampling.** The red points denote the positive samples. The center sampling strategy from FCOS takes the positive area as a square, whereas we dynamically adjust the sampling area according to the bbox shape.

$r_x, c_y + s_i \times r_y$. r_x and r_y are the horizontal and vertical radii, respectively. Considering the large difference of aspect ratio of different objects, the number of positive samples of ground-truth boxes with the same area will be greatly different if the radius is set to a fixed length. Therefore, we dynamically adjust the radius according to the aspect ratio, with the sampling radius on the longer side set to be larger, as shown in Figure 3(b). Let $f = w/h$, where w and h are the width and height of the ground-truth box, respectively. The range of f is limited between 1/1.3 and 1.3. r_x and r_y are defined as follows:

$$(r_x, r_y) = \begin{cases} (1.5 \times f, 1.5), & f > 1 \\ \left(1.5, \frac{1.5}{f}\right), & f < 1 \end{cases} \quad (1)$$

3.2 Network Outputs

As shown in Figure 2, the classification branch outputs the classification confidence with a shape as $H \times W \times C$, where C is the number of MS-COCO categories [Lin *et al.*, 2014]. The C channels of the classification outputs correspond to C binary classifiers.

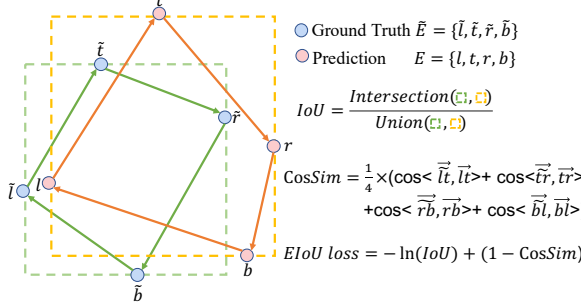


Figure 4: **Illustration of EIoU loss.** The four extreme points are taken as a convex quadrilateral composed of four vectors.

The regression branch consists of two sub-branches, which output the *EIoU* prediction results and the relative displacement vector, respectively, and their shapes are $H \times W \times 1$ and $H \times W \times 8$, respectively. Details of the *EIoU* predictor are in Chapter 3.4. Given a positive sample $P(x_p, y_p)$ and the four extreme points coordinates, the relative displacement vector is $(x_p - x_l, y_p - y_l, x_p - x_t, y_p - y_t, x_p - x_r, y_p - y_r, x_p - x_b, y_p - y_b)$. The last convolutional layer that outputs this 8D vector has no activation function because the sign of the relative displacement is uncertain.

3.3 Extreme Intersection over Union

ℓ_n -norm-based losses have the scale imbalance problem. Moreover, a gap exists between the ℓ_n -norm and the evaluation metric *IoU*. The performances of *IoU* loss and *GIoU* loss prove the effectiveness of utilizing *IoU* in regression loss. Compared with *IoU* loss, *GIoU* loss can optimize cases where bboxes have no overlap area. Therefore, we want to design a regression loss that inherits the scale-invariant property of *IoU* and can compare any two convex quadrilaterals, even for non-overlapping cases.

As shown in Figure 4, the four extreme points form an irregular convex quadrilateral. Thus, calculating the *IoU* of these two quadrilaterals seems to be optimal. However, the calculation of *IoU* with respect to non-axis-aligned quadrilaterals is very complicated. Therefore, we choose a compromise way to simplify the calculation. The features of a quadrilateral can be decomposed into position, scale, and shape. To compare the first two features, we calculate the *IoU* of the two smallest enclosing rectangles of these quadrilaterals (The dotted rectangles in Figure 4). For the last feature, we use the mean value of the cosine similarity (*CosSim*) between each paired vectors to represent the overall shape difference. The cosine similarity is equivalent to the angle between vectors, thus perfectly reflecting the shape difference.

Therefore, the similarity of any two convex quadrilaterals on the Euclidean plane can be measured by *EIoU*. As shown in Figure 4, if not specified, we use the *IoU* between the two smallest enclosing rectangles as the *IoU* in all equations. The definition of *EIoU* is shown in Equation 2.

$$EIoU = \frac{1}{2} \times (IoU + \frac{1 + \text{CosSim}}{2}) \quad (2)$$

Algorithm 1 EIoU loss Forward

Input: $\{\tilde{l}, \tilde{t}, \tilde{r}, \tilde{b}\}$ as the ground-truth.
Input: $\{x_l, y_l, \tilde{x}_t, \tilde{y}_t, \tilde{x}_r, \tilde{y}_r, \tilde{x}_b, \tilde{y}_b\}$ are their coordinates.
Input: $\{l, t, r, b\}$ as the prediction.
Input: $\{x_l, y_l, x_t, y_t, x_r, y_r, x_b, y_b\}$ are their coordinates.
Output: \mathcal{L}_{EIoU}

```

1: for each pixel (i,j) do
2:    $CosSim = \frac{1}{4} \times (\cos \langle \vec{lt}, \vec{lt} \rangle + \cos \langle \vec{tr}, \vec{tr} \rangle + \cos \langle \vec{rb}, \vec{rb} \rangle + \cos \langle \vec{bl}, \vec{bl} \rangle)$ 
3:    $EIoU loss = -\ln(IoU) + (1 - CosSim)$ 

```

The properties of *EIoU* are as follows:

1. *IoU* and cosine similarity are scale-invariant. Thus, *EIoU* also inherits this property.
2. For any two convex quadrilaterals A and B. $A, B \subseteq \mathbb{S}, 0 \leq IoU(A, B) \leq 1, -1 \leq \text{CosSim}(A, B) \leq 1$, that $0 \leq EIoU(A, B) \leq 1$ can be easily obtained. Therefore, *EIoU* is an normalized evaluation metric.
3. *IoU* can be considered a special case of *EIoU*. When both convex quadrilaterals are axis-aligned rectangles, *EIoU* is equivalent to *IoU*.

EIoU loss

With *IoU* ranges between 0 and 1, the cross-entropy loss of *IoU* is $\mathcal{L}_{IoU} = -p\ln(IoU) - (1-p)\ln(1-IoU) = -\ln(IoU)$. The range of cos similarity is between -1 and 1 and \mathcal{L}_{Cos} is defined as $1 - \text{CosSim}$. Therefore, \mathcal{L}_{EIoU} is defined as Equation 3:

$$\mathcal{L}_{EIoU} = \mathcal{L}_{IoU} + \mathcal{L}_{Cos} = -\ln(IoU) + (1 - \text{CosSim}) \quad (3)$$

The details of *EIoU* loss is shown in Algorithm 1. *EIoU* loss has the following properties:

1. *EIoU* loss is invariant to scale changes.
2. The value range of *EIoU* loss is $[0, +\infty)$. Its value will become 0 only when the two groups of extreme points completely coincide; otherwise, it will be positive. Consequently, *EIoU* loss can optimize any two groups of extreme points. The proofs are in the supplement file.



Figure 5: **Qualitative results on the val2017 split.** Extreme point and bbox detection results are on the same image. With ResNet-50 (The model with AP 39.3%), our model can achieve excellent detection results in various scenes.

Method	AP	AP ₅₀	AP ₇₅	AP _S	AP _M	AP _L
FCOS-imprv	38.7	57.7	41.7	22.0	41.3	48.5
EPP-Net	39.3	57.9	42.3	21.2	41.8	50.6
EPP-Net*	41.4	59.9	44.7	22.5	43.7	53.8

Table 1: **EPP-Net vs. FCOS.** Comparisons on the test-dev split with ResNet-50-FPN as the backbone. With the same settings as FCOS, EPP-Net performs better than FCOS and achieves an AP of 39.3%. “*” denotes using DCNv2 in heads, which boost the AP up to 41.4%.

3.4 EIoU Predictor

Here, we provide this *EIoU* predictor to deal with the mis-alignment problem between localization and classification. Object detection methods usually predict many bboxes with large overlapping areas. Therefore, the NMS algorithm is used to filter out poor prediction results with the classification confidence as the ranking keyword. However, this method may filter out the detection results with good bbox predictions but low classification confidence. Thus, our *EIoU* predictor scores each regression result by predicting the *EIoU* between each predicted bbox and its associated ground-truth. By doing so, we take the localization and classification confidence together as the evaluation criteria for prediction results.

During inference, we combine the classification confidence and the *EIoU* prediction results as the final ranking keyword in NMS, as shown in Equation 4.

$$\text{ranking} = \text{EIoU} \times \text{cls-confidence} \quad (4)$$

FCOS takes Equation 5 as the NMS ranking keyword to enhance the classification confidence from center area. However, this might filter out some high-quality prediction results from the border area. Our method takes both the classification and localization confidence as the filtering basis, which is more reasonable.

$$\text{ranking} = \text{center-ness} \times \text{cls-confidence} \quad (5)$$

3.5 Optimization

The total loss of this model is formulated as follows:

$$\mathcal{L} = \lambda_{cls} \mathcal{L}_{cls} + \lambda_{reg} \mathcal{L}_{reg} + \lambda_{eIoU-p} \mathcal{L}_{eIoU-p} \quad (6)$$

loss	AP	AP ₅₀	AP ₇₅	AP _S	AP _M	AP _L
Smooth- ℓ_1	39.3	58.9	42.6	21.8	41.1	50.9
<i>EIoU</i> loss	40.7	59.5	44.0	22.4	42.7	53.0

Table 2: **EIoU loss vs. Smooth- ℓ_1 loss.** Settings are the same as the EPP-Net* in Table 1. The performance of *EIoU* loss is much better than that of Smooth- ℓ_1 loss.

<i>EIoU</i> ^{pre}	<i>Ctr</i> ^{pre}	<i>EIoU</i> ^{nms}	<i>Ctr</i> ^{nms}	\ominus ^{nms}	AP
○	✓	○	✓	○	40.7
✓	✓	○	✓	○	41.2
✓	✓	○	○	✓	40.6
✓	✓	✓	○	○	41.4

Table 3: **EIoU vs. Center-ness.** Settings are the same as the EPP-Net* in Table 1. *EIoU*^{pre} and *Ctr*^{pre} denote the *EIoU* predictor and the center-ness predictor, respectively. *EIoU*^{nms}, *Ctr*^{nms} and \ominus ^{nms} denote using Equation 4, 5 and the raw classification confidence as the ranking keyword in NMS.

\mathcal{L}_{cls} is focal loss for classification as in [Lin *et al.*, 2017b], and \mathcal{L}_{reg} is defined in Equation 3. \mathcal{L}_{eIoU-p} is BCE loss for *EIoU* predictions. To balance losses of all subtasks, hyper-parameters λ_{cls} , λ_{reg} , and λ_{eIoU-p} are all set as 1.

4 Experiments

In this section, we perform several experiments on the MS-COCO dataset [Lin *et al.*, 2014] to show the effectiveness of EPP-Net and its components. EPP-Net is trained on the COCO train2017 split (115K images) and evaluated on the test-dev split (20K images) for the ablation study. Visualization experiments are conducted on the val2017 split (5K images). We also upload the detection results on test-dev with different backbones to the MS-COCO server to compare our EPP-Net with recent state-of-the-art detectors.

4.1 Implementation Details

Extreme points are computed from the polygonal mask annotations following the extraction strategy from [Zhou *et al.*, 2019]. The hyperparameters in our model follow those in FCOS, and we use pre-trained models on ImageNet to ini-

Method	Backbone	AP	AP ₅₀	AP ₇₅	AP _S	AP _M	AP _L
Anchor-Based							
Faster R-CNN w/ FPN [Lin <i>et al.</i> , 2017a]	ResNet-101	36.2	59.1	39.0	18.2	39.0	48.2
RetinaNet [Lin <i>et al.</i> , 2017b]	ResNeXt-101	40.8	61.1	44.1	24.1	44.2	51.2
IoU-Net [Jiang <i>et al.</i> , 2018]	ResNet-101	40.6	59.0	-	-	-	-
YOLOv4 [Bochkovskiy <i>et al.</i> , 2020]	CSPDarknet-53	43.5	65.7	47.3	26.7	46.7	53.3
Anchor-Free							
CornerNet [Law and Deng, 2018]	Hourglass-104	40.5	59.1	42.3	21.8	42.7	50.2
ExtremeNet [Zhou <i>et al.</i> , 2019]	Hourglass-104	40.2	55.5	43.2	20.4	43.2	53.1
FoveaBox-align [Kong <i>et al.</i> , 2020]	ResNeXt-101	43.9	63.5	47.7	26.8	46.9	55.6
FCOS-imprv [Tian <i>et al.</i> , 2019]	ResNeXt-101	44.7	64.1	48.4	27.6	47.5	55.6
EPP-Net	ResNeXt-101	45.1	64.4	48.9	26.8	48.5	56.1
EPP-Net	ResNeXt-101-DCN	48.3	67.5	52.5	29.0	51.6	61.6

Table 4: **EPP-Net vs. State-of-the-art Detectors.** “DCN” denotes using DCNv2 in backbone and heads; otherwise, no DCNv2 in the network. EPP-Net outperforms anchor-based and anchor-free detectors.

talize network weights. If not specified, we use ResNet-50 and feature pyramid network as our basic network. We train this network with stochastic gradient descent and a total batch size of 16 images on 8 NVIDIA TITAN RTX GPUs for 180K iterations. We set the initial learning rate as 0.01, and the momentum and the weight decay as 0.9 and 0.0001, respectively. We decrease the learning rate by 10 at epochs 16 and epoch 22. The *IoU* threshold in NMS is set as 0.6.

4.2 Ablation Study

We perform several groups of ablation experiments to validate the effectiveness of different components. All test results are reported on MS-COCO test-dev split.

Overall performance. We compare our method with FCOS to evaluate the overall performance of EPP-Net. As shown in Table 1, the comparison reveals that EPP-Net outperforms FCOS with an AP of 39.3%. We observe a considerable improvement of AP in large objects, namely, 2.1%. We explain as follows: First, the extreme point training annotations are computed from instance segmentation annotations, whereas the testing ground-truth is from bbox annotations. However, the extreme points and the bbox do not coincide completely, with a slight misalignment between them. The smaller the objects are, the larger the relative misalignment. Therefore, this testing method is unfair to our model. Second, the shape variance of larger objects is larger than that of small objects, and this problem can be well solved by extreme point prediction because its supervision is more explicit than the bbox. The detection results are shown in Figure 5. We also apply DCNv2 [Zhu *et al.*, 2019b] in heads to improve EPP-Net and achieve a 2.1% performance improvement.

EIoU loss. We take Smooth- ℓ_1 loss and *EIoU* loss as the regression loss, respectively, to prove the effectiveness of *EIoU* loss. For a fair comparison, we replace the *EIoU* predictor with center-ness predictor and use Equation 5 as the ranking keyword in NMS. The results are shown in Table 2. *EIoU* loss achieves an AP of 40.7%, which outperforms Smooth- ℓ_1 loss by 1.4%. AP_S, AP_M, and AP_L are all raised considerably, which proves the importance of the scale invariance property of regression loss.

EIoU predictor and EIoU-guided NMS. To compare the effectiveness of *EIoU* and center-ness predictors. We append both predictors on the regression branch and take Equation 4, 5 and the raw classification confidence as the ranking keyword in NMS, respectively. As shown in Table 3, surprisingly, the AP raised from 40.7% to 41.2% with the addition of the *EIoU* predictor. After using the predicted *EIoU* as the ranking keyword instead of center-ness, the AP is improved by 0.2%. If using traditional NMS, the AP is reduced to 40.6%. We can conclude that both the *EIoU* predictor and the *EIoU*-guided NMS can improve the detection accuracy.

4.3 State-of-the-art Comparisons

Table 4 shows the comparison results between EPP-Net and state-of-the-art detectors. We use multi-scale training with the shorter side of input images randomly resized from 640 to 800 and the longer side less than 1333. Test results are reported on the MS-COCO test-dev split. Our model achieves a substantial improvement with different backbones. Compared with anchor-based RetinaNet, our model achieves an improvement of 4.3% in AP with backbone ResNeXt-101. EPP-Net also outperforms key-point-based detectors, CornerNet and ExtremeNet, with better accuracy and without the grouping process. Moreover, EPP-Net outperforms dense detector FCOS and achieves an AP of 45.1% with the same backbone. Finally, the performance of the best model reaches 48.3% AP with ResNeXt-101-DCN as the backbone.

5 Conclusion

In this paper, we present EPP-Net as a new method to detect an object by predicting the relative displacement vector between each location and the four extreme points. We also propose *EIoU*, a novel evaluation metric, to measure the similarity between two groups of extreme points. Moreover, our proposed *EIoU* loss can deal with the scale imbalance problem, which outperforms Smooth- ℓ_1 loss. Furthermore, we propose the *EIoU* predictor and *EIoU*-guided NMS, which help the detector obtain better localization results. The detection results on the MS-COCO reveal that our method can achieve state-of-the-art accuracy. As for future work, our architecture will be extended to pose estimation.

References

[Bochkovskiy *et al.*, 2020] Alexey Bochkovskiy, Chien-Yao Wang, and Hong-Yuan Mark Liao. Yolov4: Optimal speed and accuracy of object detection. *arXiv preprint arXiv:2004.10934*, 2020.

[Duan *et al.*, 2019] Kaiwen Duan, Song Bai, Lingxi Xie, Honggang Qi, Qingming Huang, and Qi Tian. Centernet: Keypoint triplets for object detection. In *Proceedings of the IEEE International Conference on Computer Vision*, pages 6569–6578, 2019.

[He *et al.*, 2017] Kaiming He, Georgia Gkioxari, Piotr Dollár, and Ross Girshick. Mask r-cnn. In *Proceedings of the IEEE international conference on computer vision*, pages 2961–2969, 2017.

[Huang *et al.*, 2015] Lichao Huang, Yi Yang, Yafeng Deng, and Yinan Yu. Densebox: Unifying landmark localization with end to end object detection. *arXiv preprint arXiv:1509.04874*, 2015.

[Jiang *et al.*, 2018] Borui Jiang, Ruixuan Luo, Jiayuan Mao, Tete Xiao, and Yuning Jiang. Acquisition of localization confidence for accurate object detection. In *Proceedings of the European Conference on Computer Vision (ECCV)*, pages 784–799, 2018.

[Kong *et al.*, 2020] Tao Kong, Fuchun Sun, Huaping Liu, Yuning Jiang, Lei Li, and Jianbo Shi. Foveabox: Beyond anchor-based object detection. *IEEE Transactions on Image Processing*, 29:7389–7398, 2020.

[Law and Deng, 2018] Hei Law and Jia Deng. Cornernet: Detecting objects as paired keypoints. In *Proceedings of the European Conference on Computer Vision (ECCV)*, pages 734–750, 2018.

[Lin *et al.*, 2014] Tsung-Yi Lin, Michael Maire, Serge Belongie, James Hays, Pietro Perona, Deva Ramanan, Piotr Dollár, and C Lawrence Zitnick. Microsoft coco: Common objects in context. In *European conference on computer vision*, pages 740–755. Springer, 2014.

[Lin *et al.*, 2017a] Tsung-Yi Lin, Piotr Dollár, Ross Girshick, Kaiming He, Bharath Hariharan, and Serge Belongie. Feature pyramid networks for object detection. In *Proceedings of the IEEE conference on computer vision and pattern recognition*, pages 2117–2125, 2017.

[Lin *et al.*, 2017b] Tsung-Yi Lin, Priya Goyal, Ross Girshick, Kaiming He, and Piotr Dollár. Focal loss for dense object detection. In *Proceedings of the IEEE international conference on computer vision*, pages 2980–2988, 2017.

[Long *et al.*, 2015] Jonathan Long, Evan Shelhamer, and Trevor Darrell. Fully convolutional networks for semantic segmentation. In *Proceedings of the IEEE conference on computer vision and pattern recognition*, pages 3431–3440, 2015.

[Qiu *et al.*, 2020] Han Qiu, Yuchen Ma, Zeming Li, Songtao Liu, and Jian Sun. Borderdet: Border feature for dense object detection. In *European Conference on Computer Vision*, pages 549–564. Springer, 2020.

[Redmon and Farhadi, 2017] Joseph Redmon and Ali Farhadi. Yolo9000: better, faster, stronger. In *Proceedings of the IEEE conference on computer vision and pattern recognition*, pages 7263–7271, 2017.

[Redmon *et al.*, 2016] Joseph Redmon, Santosh Divvala, Ross Girshick, and Ali Farhadi. You only look once: Unified, real-time object detection. In *Proceedings of the IEEE conference on computer vision and pattern recognition*, pages 779–788, 2016.

[Ren *et al.*, 2016] Shaoqing Ren, Kaiming He, Ross Girshick, and Jian Sun. Faster r-cnn: Towards real-time object detection with region proposal networks. *IEEE transactions on pattern analysis and machine intelligence*, 39(6):1137–1149, 2016.

[Rezatofighi *et al.*, 2019] Hamid Rezatofighi, Nathan Tsoi, JunYoung Gwak, Amir Sadeghian, Ian Reid, and Silvio Savarese. Generalized intersection over union: A metric and a loss for bounding box regression. In *Proceedings of the IEEE Conference on Computer Vision and Pattern Recognition*, pages 658–666, 2019.

[Song *et al.*, 2020] Guanglu Song, Yu Liu, and Xiaogang Wang. Revisiting the sibling head in object detector. In *Proceedings of the IEEE/CVF Conference on Computer Vision and Pattern Recognition*, pages 11563–11572, 2020.

[Tian *et al.*, 2019] Zhi Tian, Chunhua Shen, Hao Chen, and Tong He. Fcos: Fully convolutional one-stage object detection. In *Proceedings of the IEEE/CVF International Conference on Computer Vision (ICCV)*, October 2019.

[Wojke *et al.*, 2017] Nicolai Wojke, Alex Bewley, and Dieterich Paulus. Simple online and realtime tracking with a deep association metric. In *2017 IEEE international conference on image processing (ICIP)*, pages 3645–3649. IEEE, 2017.

[Yu *et al.*, 2016] Jiahui Yu, Yuning Jiang, Zhangyang Wang, Zhimin Cao, and Thomas Huang. Unitbox: An advanced object detection network. In *Proceedings of the 24th ACM international conference on Multimedia*, pages 516–520, 2016.

[Zhou *et al.*, 2019] Xingyi Zhou, Jiacheng Zhuo, and Philipp Krahenbuhl. Bottom-up object detection by grouping extreme and center points. In *Proceedings of the IEEE Conference on Computer Vision and Pattern Recognition*, pages 850–859, 2019.

[Zhu *et al.*, 2019a] Chenchen Zhu, Yihui He, and Marios Savvides. Feature selective anchor-free module for single-shot object detection. In *Proceedings of the IEEE Conference on Computer Vision and Pattern Recognition*, pages 840–849, 2019.

[Zhu *et al.*, 2019b] Xizhou Zhu, Han Hu, Stephen Lin, and Jifeng Dai. Deformable convnets v2: More deformable, better results. In *Proceedings of the IEEE Conference on Computer Vision and Pattern Recognition*, pages 9308–9316, 2019.